

Improved foreground removal in GMRT 610 MHz observations towards redshifted 21-cm tomography

Abhik Ghosh^{1*}, Somnath Bharadwaj^{1†}, Sk. Saiyad Ali^{2‡} and

Jayaram N. Chengalur^{3§}

¹ *Department of Physics and Meteorology & Centre for Theoretical Studies, IIT Kharagpur, 721 302, India*

² *Department of Physics, Jadavpur University, Kolkata 700032, India.*

³ *National Centre for Radio Astrophysics, TIFR, Post Bag 3, Ganeshkhind, Pune 411 007, India*

ABSTRACT

Foreground removal is a challenge for 21-cm tomography of the high redshift Universe. We use archival GMRT data (obtained for completely different astronomical goals) to estimate the foregrounds at a redshift ~ 1 . The statistic we use is the cross power spectrum between two frequencies separated by $\Delta\nu$ at the angular multipole ℓ , or equivalently the multi-frequency angular power spectrum $C_\ell(\Delta\nu)$. An earlier measurement of $C_\ell(\Delta\nu)$ using this data had revealed the presence of oscillatory patterns along $\Delta\nu$, which turned out to be a severe impediment for foreground removal (Ghosh et al. 2011). Using the same data, in this paper we show that it is possible to considerably reduce these oscillations by suppressing the sidelobe response of the primary antenna elements. The suppression works best at the angular multipoles ℓ for which there is a dense sampling of the u-v plane. For three angular multipoles $\ell = 1405, 1602$ and 1876 , this sidelobe suppression along with a low order polynomial fitting completely results in residuals of ($\leq 0.02 \text{ mK}^2$), consistent with the noise at the 3σ level. Since the polynomial fitting is done after estimation of the power spectrum it can be ensured that the estimation of the HI signal is not biased. The corresponding 99% upper limit on the HI signal is $\bar{x}_{\text{HI}} b \leq 2.9$, where \bar{x}_{HI} is the mean neutral fraction and b is the bias.

Key words: techniques:interferometric-radio continuum:general-(cosmology:) diffuse radiation

1 INTRODUCTION

Observations of redshifted 21 cm radiation from neutral hydrogen (HI) hold the potential of tracing the large scale structure of the Universe over a large redshift range ($20 \geq z \geq 0$). This signal ($\sim \text{mK}$), is however, buried in the emission from other astrophysical sources which are collectively referred to as foregrounds. These foregrounds are dominated by the extragalactic radio sources, the diffuse synchrotron radiation from our own Galaxy (GDSE) and a smaller contribution comes from galactic free-free emission (Shaver et al. 1999). The extragalactic point sources have a typical spectral index of $\beta \sim -0.8$ (Subrahmanyan 2002), with evidence of flattening at lower frequencies (Cohen et al. 2004). The analysis of radio surveys at 408 MHz, 1.42 GHz, and

2.326 GHz (Haslam et al. 1982; Reich 1982; Reich & Reich 1988; Jonas, Baart, & Nicolson 1998) show that the GDSE has a steep spectral index to be $\alpha \approx -2.8$. This is also in broad agreement with the results presented in Platania et al. (1998). Di Matteo et al. (2002) have used the 6C survey (Hales, Baldwin & Warner 1988), and the 3CR survey and the 3 CRR catalogue (Laing, Riley & Longair 1983) to estimate the resolved extragalactic radio sources (point sources) contribution at 150 MHz. Recently Bernardi et al. (2009) have characterized the power spectrum of the total diffuse radiation at 150 MHz at the angular scales of our interest. Separating the redshifted HI signal from the foregrounds, which are several order of magnitude larger (e.g. Shaver et al. 1999; Di Matteo et al. 2002), is currently the biggest challenge for 21-cm tomography of the high redshift Universe. The problem, in principle, can be solved using the fact that the redshifted 21-cm signals at two different frequencies ν and $\nu + \Delta\nu$ are expected to be uncorrelated at separations $\Delta\nu \geq 0.5 \text{ MHz}$ at the angular scales of our

* E-mail: abhik@phy.iitkgp.ernet.in

† Email:somnath@phy.iitkgp.ernet.in

‡ Email:saiyad@phys.jdvu.ac.in

§ Email:chengalu@ncra.tifr.res.in

interest whereas the foregrounds, which arise from continuum sources, are expected to remain correlated over considerably large frequency separations (Bharadwaj & Sethi 2001; Di Matteo et al. 2002; Oh and Mack 2003; Di Matteo et al. 2004; Zaldarriaga, Furlanetto & Hernquist 2004; Morales & Hewitt 2004; Bharadwaj and Ali 2005; Santos et al. 2005; Wang et al. 2006). We note that the prospects of detecting the redshifted 21-cm HI signal are considerably better at higher frequencies (e.g., 610 MHz) which probe the post-reionization era ($z < 6$) in comparison to the lower frequencies (e.g., 150 MHz) which probe the reionization era. Further, the problem of man made radio frequency interference (hereafter RFI) is considerably less severe at higher frequencies.

In this paper we report a substantial improvement in foreground removal in the context of our earlier work (Ghosh et al. 2011, hereafter Paper I) which presents Giant Metrewave Radio Telescope (GMRT¹ Swarup et al. 1991) 610 MHz observations towards detecting the post-reionization 21-cm signal from $z = 1.32$. In Paper I we have determined, possibly for the first time, the statistical properties of the background radiation over the angular scales $20''$ to $10'$ and a frequency band of 7.5 MHz centered at 616.25 MHz. The analysis was carried out using the multi-frequency angular power spectrum (MAPS) $C_\ell(\Delta\nu)$ (Datta, Roy Choudhury & Bharadwaj 2007) which jointly characterizes the angular ℓ and frequency $\Delta\nu$ dependence of the fluctuations in the background radiation. The measured $C_\ell(\Delta\nu)$, which ranges from 7 mK^2 to 18 mK^2 , is dominated by foregrounds, the expected HI signal being several orders of magnitude smaller ($C_\ell^{\text{HI}}(\Delta\nu) \sim 10^{-6} - 10^{-7} \text{ mK}^2$). The measured signal, for a fixed ℓ , is expected to vary smoothly with $\Delta\nu$ and remain nearly constant over the observational bandwidth. We find instead that in addition to a component that exhibits a smooth $\Delta\nu$ dependence, the measured $C_\ell(\Delta\nu)$ also has a component that oscillates as a function of $\Delta\nu$. The amplitude of the oscillating component is around 1 – 4% of the smooth component, and the amplitude and period of oscillation both decreases with increasing ℓ . We note that similar oscillations, with considerably larger amplitudes, have been reported in GMRT observations at 153 MHz (Ali, Bharadwaj & Chengalur 2008) which is relevant for the signal from the reionization era. The origin of the oscillatory signal was unclear.

The oscillatory patterns pose a serious obstacle for foreground removal (Paper I). It is thus important to identify the cause (or causes) and implement techniques to mitigate the oscillatory patterns. The fact that the primary beam (hereafter PB) pattern changes with frequency across the observational bandwidth, not included in our previous analysis (Paper I), could be a possible cause. In particular, the angular position of the nulls and the side-lobes changes with frequency, and a bright continuum source located near the null or located in the sidelobes will be seen as oscillations along the frequency axis in the measured visibilities. It is thus quite plausible that bright sources located near the null or the sidelobes of the PB produce the oscillatory pattern in the measured $C_\ell(\Delta\nu)$ which is estimated from correlations amongst the visibilities. One can, in principle, design anten-

nas with a frequency-dependent collecting area to produce a nearly constant PB pattern. However, to our knowledge, none of the upcoming arrays have this feature and we expect this issue to be relevant not only for the GMRT but for all the arrays planned in the near future.

The problem can be mitigated by tapering the array's sky response with a frequency independent window function $W(\vec{\theta})$ that falls off before the first null of the PB pattern and thereby suppresses the sidelobe response. It is simplest to implement this by multiplying the sky image $I(\vec{\theta})$ with $W(\vec{\theta})$ and using a Fourier transform of this to recalculate the visibilities. This, however, will introduce correlations between the noise in the recalculated visibilities which is a nuisance for estimating $C_\ell(\Delta\nu)$. The other option is to work entirely with the visibilities in the $u-v$ plane, avoiding the need for an image. In this approach the sky response is tapered by convolving the visibilities with $\bar{W}(\vec{U})$ - the Fourier transform of $W(\vec{\theta})$. As we show later in this paper, it is possible to implement the convolution without introducing a noise bias in the estimated $C_\ell(\Delta\nu)$. We note that convolving the visibilities with a "gridding convolution function" has long been a standard practice while making images from interferometric data (Section 3., Sramek & Schwab 1989). This convolution is done to avoid aliasing which would otherwise occur when one uses an FFT to make the image. As discussed in detail by Sramek & Schwab (1989) the convolution function is generally chosen to provide an optimum balance between alias rejection and ease of computation. The focus here is somewhat different, viz. to use the convolution to strongly attenuate the frequency dependent response to the sidelobes of the primary antenna pattern.

RFI sources, which are mostly located on the ground, are picked up through the sidelobes. Suppressing the sidelobe response is also expected to mitigate the RFI contribution.

Paper I contains a detailed description of the data, we mention a few salient features here. The data is taken from an archival 30 hours observation centered on $\alpha_{2000} = 12^{\text{h}}36^{\text{m}}49^{\text{s}}$, $\delta_{2000} = 62^{\circ}17'57''$ which is situated near Hubble Deep Field North (HDF-N). For the present work we have analyzed the frequency range 612.5 MHz to 620.0 MHz with channels 125 kHz wide. Visibilities were recorded for two orthogonal circular polarizations with 16s integration time. Calibration was carried out using standard AIPS tasks, and the visibilities from the two polarizations were combined ($\mathcal{V} = [\mathcal{V}_{RR} + \mathcal{V}_{LL}]/2$) for the rest of the analysis.

2 SIDELOBE SUPPRESSION

The observed visibilities $\mathcal{V} = \tilde{a} \otimes \tilde{I}$ record the Fourier transform of the sky brightness \tilde{I} convolved with the antenna aperture \tilde{a} . The frequency dependence and the sidelobes come in through $\tilde{a}(\mathbf{U}, \nu)$ whose Fourier transform gives the PB pattern $A(\vec{\theta}, \nu)$. Close to the phase centre, the PB is reasonably well modeled by a Gaussian $A(\vec{\theta}, \nu) = e^{-\theta^2/\theta_0^2}$ where the parameter θ_0 is related to the FWHM of the PB as $\theta_0 \approx 0.6 \times \theta_{\text{FWHM}}$, and $\theta_0 = 25'.8$ ($\theta_{\text{FWHM}} = 43'$) at 610 MHz for the GMRT with $\theta_0 \propto \nu^{-1}$. Note that the Gaussian model for $A(\vec{\theta}, \nu)$ breaks down away from the phase center where we have the sidelobes and nulls.

¹ <http://www.gmrt.ncra.tifr.res.in>

We mitigate the effect of the frequency dependent sidelobe pattern by convolving the observed visibilities with a suitably chosen function $\tilde{W}(\mathbf{U})$. The sky response of the convolved visibilities $\mathcal{V}_c = \tilde{W} \otimes \mathcal{V}$ is modulated by the window function $W(\vec{\theta})$ which is the Fourier transform of $\tilde{W}(\mathbf{U})$. We have used a window function $W(\vec{\theta}) = e^{-\theta^2/\theta_w^2}$ with $\theta_w < \theta_0$ to taper the sky response so that it falls off well before the sidelobes. Note that θ_w and $W(\vec{\theta})$ are both frequency independent. We parametrize θ_w as $\theta_w = f\theta_0$ with $f \leq 1$ where θ_0 here refers to the value at the fixed frequency 610 MHz.

We can evaluate the convolved visibilities \mathcal{V}_c on a grid in $u - v$ space ($\mathcal{V}_c(\mathbf{U}_i, \nu) = \sum_a \tilde{W}(\mathbf{U}_i - \mathbf{U}_a) \mathcal{V}(\mathbf{U}_a, \nu)$) and use these to determine the two-visibility correlation defined as $V_2(\mathbf{U}_i, \Delta\nu) = \mathcal{V}_c(\mathbf{U}_i, \nu) \mathcal{V}_c^*(\mathbf{U}_i, \nu + \Delta\nu)$. Here $\mathbf{U} \equiv (u, v)$ refers to a two-dimensional baseline, \mathbf{U}_i refers to points on the grid in $u - v$ space and \mathbf{U}_a refers to the different baselines in the observational data. This way of estimating $V_2(\mathbf{U}_i, \Delta\nu)$, however, introduces a positive noise bias (e.g. Begum et al. (2006)) which is not desirable. We use, instead, the estimator $V_2(\mathbf{U}_i, \Delta\nu) = K^{-1} \times \sum_{a \neq b} [\tilde{W}(\mathbf{U}_i - \mathbf{U}_a) \tilde{W}^*(\mathbf{U}_i - \mathbf{U}_b) \mathcal{V}(\mathbf{U}_a, \nu) \mathcal{V}^*(\mathbf{U}_b, \nu + \Delta\nu)]$, where $K = \sum_{a \neq b} \tilde{W}(\mathbf{U}_i - \mathbf{U}_a) \tilde{W}^*(\mathbf{U}_i - \mathbf{U}_b)$ is a normalization constant. The noise bias is avoided by dropping the self-correlations (*i.e.* the terms with $a = b$). We have used a grid of spacing $\Delta U_g = \sqrt{\ln 2}/(\pi\theta_w) = 0.265\theta_w^{-1}$ which corresponds to half of the FWHM of $\tilde{W}(\mathbf{U})$, and we have estimated $V_2(\mathbf{U}_i, \Delta\nu)$ at every grid point using all the baselines within a disk of radius $2\Delta U_g$ centered on that grid point. We finally determine $C_\ell(\Delta\nu)$ using (Ali, Bharadwaj & Chengalur 2008)

$$V_2(U, \Delta\nu) = \frac{\pi\theta'^2}{2} \left(\frac{\partial I_\nu}{\partial T} \right)^2 C_\ell(\Delta\nu) Q(\Delta\nu). \quad (1)$$

where $\ell = 2\pi U$, $\theta'^{-2} = \theta_0^{-2} + \theta_w^{-2}$ and $Q(\Delta\nu)$ is a slowly varying function of $\Delta\nu$ which accounts for the fact that we have treated θ'^2 and $(\partial I_\nu/\partial T)$ as constants in our analysis. We have used $Q(\Delta\nu) = 1$ which introduces an extra $\Delta\nu$ dependence in the estimated $C_\ell(\Delta\nu)$. This, we assume, will be a small effect and can be accounted for during foreground removal. The data has been binned assuming that the statistical properties of the signal are isotropic in \mathbf{U} .

2.1 Simulation

In order to demonstrate the efficacy of our technique of sidelobe suppression using a simulated data set, the GMRT antenna was modeled as a circular aperture of $D = 45$ m diameter with a circular disk of diameter $D_1 = 1$ m at the center blocked due to the feed. This gives a normalized antenna beam pattern

$$A_\nu(\theta) = \frac{4}{(D^2 - D_1^2)^2} \left[D^2 \frac{J_1(\pi\theta D/\lambda)}{(\pi\theta D/\lambda)} - D_1^2 \frac{J_1(\pi\theta D_1/\lambda)}{(\pi\theta D_1/\lambda)} \right]^2 \quad (2)$$

where J_1 is the Bessel function of the first kind of order one. Several point sources were randomly placed in the region near fifth null of this beam pattern. The expected number of point sources and their flux distribution can be predicted from the differential source counts (Garn, Green, Riley et al. 2008). Given that the present simulation has the limited aim of demonstrating the efficiency of our sidelobe suppression technique, we have instead used a cartoon model with five

hundred point sources each having the same flux density 150 mJy. The value of the flux density was chosen so that the simulated $C_\ell(\Delta\nu)$ has a value around ~ 10 mK², comparable to our measured $C_\ell(\Delta\nu)$ (Figure 7, Paper I).

Next, we have randomly generated baselines, and calculated the corresponding visibilities for the five-hundred point sources. It may be noted that the simulated baselines have a density of 0.3/m² which is roughly consistent with the GMRT central square. The antenna beam pattern (eq. 2) was used in calculating the simulated visibilities. We have used the simulated visibilities to estimate $C_\ell(\Delta\nu)$. Then, we have fitted a third order polynomial in $\Delta\nu$ to subtract out the component of the sky signal that varies slowly with frequency. The residual $C_\ell(\Delta\nu)$ has an oscillatory pattern with amplitude ($\sim 10^{-2}$ mK²). The procedure was repeated after introducing a convolution with $f = 0.8$. This tapers the sky response to $\sim 0.8\%$ of its peak value at the first null of the beam and considerably reduces the response to the sources beyond the first null. We find that the residuals, after polynomial subtraction, are in the range 10^{-5} mK² to 10^{-4} mK², *i.e.* the residuals are suppressed by a factor of around 10^2 to 10^3 . Further, after convolution the residuals appear to be noise like and do not show any noticeable oscillatory feature. Note that although we have shown results of our simulation for only a single ℓ value, the results are very similar at other ℓ values.

3 RESULTS AND CONCLUSIONS

We first investigate whether sidelobe suppression at all helps to reduce the oscillations that were reported in Paper I. This is quantified using the dimensionless decorrelation function $\kappa_\ell(\Delta\nu) = C_\ell(\Delta\nu)/C_\ell(0)$. We have considered $f = 0.4, 0.65$ and 0.8 which respectively correspond to a tapered sky response with FWHM 17'.2, 28'.0 and 34'.4 as compared to the GMRT PB which has a FWHM of 43' at 610 MHz. The results are shown in Figure 2 for the four smallest ℓ values for which we have measured the binned $C_\ell(\Delta\nu)$. The oscillatory patterns are distinctly visible in the cases where the tapering has not been applied. We see that in most cases the oscillations are considerably reduced and are nearly absent when tapering is applied. We do not, however, notice any particular qualitative trend with varying f . The oscillatory pattern with a large period in $\Delta\nu$ seen at $\ell = 1405$, the smallest ℓ value, persists even after the tapering is applied. This, however, does not pose a problem for foreground removal as the $C_\ell(\Delta\nu)$, after tapering, is well fitted by a low order polynomial and can be successfully removed.

The tapering, which has been implemented through a convolution, is expected to be most effective in a situation where the $u - v$ space is densely sampled by the baseline distribution. Our results are limited by the patchy $u - v$ coverage of the present observational data. This also possibly explains why the oscillations persist after tapering at the smallest ℓ value. Tapering the the field of view has a drawback in that this increases the cosmic variance which scales as f^{-1} . It is possible to compensate for this by repeating the entire analysis after adding phases to the visibilities so as to shift the center of the field of view. We have not attempted this here, and our entire analysis is restricted to a single field of view. The increase in the cosmic variance

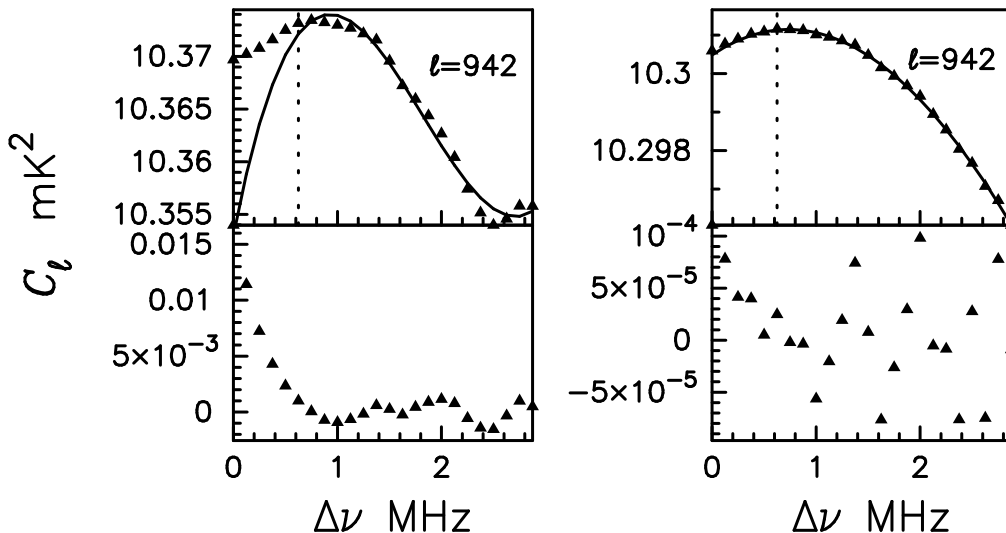


Figure 1. The data points in the top panels show $C_\ell(\Delta\nu)$ estimated without (left) and with (right) sidelobe suppression. The solid lines show the respective best fit polynomials used for foreground subtraction. The residuals, after foreground subtraction, are shown in the corresponding bottom panels.

can also be used as a guiding principle in choosing the value of f . It is most advantageous to use the smallest value of f where the oscillations are adequately suppressed. Of the three values of f that we have considered here, we find that foreground subtraction is most effective for $f = 0.65$, and we use this for the entire subsequent analysis.

The measured $C_\ell(\Delta\nu)$ shown in Figure 3 is foreground dominated and it is seen to vary smoothly with increasing $\Delta\nu$. On the contrary, the predicted contribution from the HI signal $C_\ell^{\text{HI}}(\Delta\nu)$ decreases very rapidly with increasing $\Delta\nu$ (Bharadwaj & Sethi 2001). We have used a polynomial fitting technique (Paper I) to identify and subtract out any smoothly varying component from the measured $C_\ell(\Delta\nu)$ and thereby remove the foreground contribution. The possibility that along with the foregrounds the fitting procedure may also remove a part of the signal is a major concern. For each ℓ value we have estimated $\Delta\nu_{0.1}$ which corresponds to the frequency separation where $C_\ell^{\text{HI}}(\Delta\nu)$ first falls to less than 10% of the peak value $C_\ell^{\text{HI}}(0)$. The bulk of the HI signal is localized within $\Delta\nu < \Delta\nu_{0.1}$ which is excluded when estimating the slowly varying foreground contribution. We have used the range $\Delta\nu_{0.1} \leq \Delta\nu \leq 6 \times \Delta\nu_{0.1}$ to estimate the coefficients of the best fit 4th order polynomial and we use this to subtract out the foreground contribution from the entire range $\Delta\nu \leq 6 \times \Delta\nu_{0.1}$. The value of $\Delta\nu_{0.1}$ and the polynomial fit are both shown in Figure 3. Note that $\Delta\nu_{0.1}$ decreases with increasing ℓ , and it is less than 0.5 MHz for all the ℓ values that we have considered. Tests with simulations (Paper I) show that very little of the HI signal is lost in this subtraction procedure.

It is noteworthy that a variety of foreground removal techniques (e.g. McQuinn et al. 2006; Jelić et al. 2008; Gleser et al. 2008; Harker et al. 2009; Liu, Tegmark & Zaldarriaga 2009; Liu et al. 2009; Petrovic & Oh 2011) all attempt to remove the foregrounds from images or visibilities *before* determining the power spectrum. The HI signal is spread out along the entire frequency axis and all these techniques run the risk of removing a part of the HI signal along with the foregrounds. On the contrary, we have attempted foreground

removal *after* determining the angular power spectrum. The signal, here, is localized in $\Delta\nu$, and it is possible to reduce the risk of removing a part of the HI signal by suitably tuning the fitting procedure.

We expect the residual $C_\ell^{\text{RES}}(\Delta\nu)$ that remains after polynomial subtraction (Figure 4) to contain only the HI signal and noise provided the foregrounds have been successfully removed. In our observations the HI signal is much smaller than the noise $\sigma \sim 0.01 \text{ mK}^2$. We thus expect the residuals to be consistent with noise provided the foregrounds have been completely removed. We find that the residuals are consistent with noise at the 3σ level (*ie.* $C_\ell^{\text{RES}}(\Delta\nu) \leq 0 \pm 3\sigma$) at the three smallest values of ℓ (1405, 1602, 1876). This establishes that our foreground removal technique works. This technique, however, is not as successful at $\ell = 2214$ where a single point of $\Delta\nu = 0$ has a value that is somewhat larger than $0 \pm 3\sigma$. We have also carried out the entire analysis for several other, larger, values of ℓ for which the results have not been shown here. While sidelobe suppression works quite well in removing the oscillations, we are unable to completely remove the foregrounds for the other ℓ values.

The fact that we have three ℓ values where the foregrounds have been completely removed and $C_\ell^{\text{RES}}(\Delta\nu)$ is consistent with noise allows us to place an upper limit on the HI signal. We assume that the HI traces the dark matter with a possible linear bias b whereby $C_\ell^{\text{HI}}(\Delta\nu)$ can be calculated (Paper I) in terms of the dark matter power spectrum, and the cosmological parameters for which we have used the values $(\Omega_{m0}, \Omega_{\Lambda0}, h, \sigma_8, n_s) = (0.3, 0.7, 0.7, 1.0, 1.0)$. The HI signal is now completely determined upto a proportionality factor $C_\ell^{\text{HI}}(\Delta\nu) \propto [\bar{x}_{\text{HI}}b]^2$ where \bar{x}_{HI} is the mean neutral fraction of hydrogen gas. We have considered $\bar{x}_{\text{HI}}b$ as a free parameter, and performed a likelihood analysis using our observational data to place an upper limit on $\bar{x}_{\text{HI}}b$. In our analysis we have assumed that the $C_\ell(\Delta\nu)$ at the different ℓ values are independent. For each ℓ , we have only used $C_\ell(\Delta\nu)$ in the range $\Delta\nu < \Delta\nu_{0.1}$; the $\Delta\nu$ values that were used to estimate the polynomial for foreground removal were

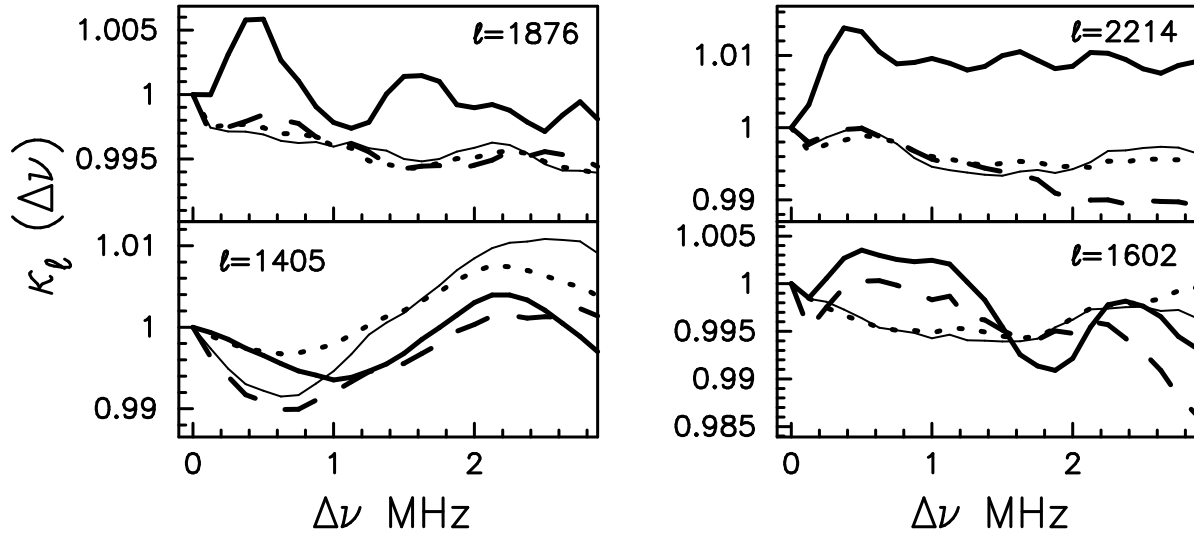


Figure 2. The measured $\kappa_\ell(\Delta\nu)$ as a function of $\Delta\nu$ for the ℓ value as shown in each panel. The results from our earlier analysis (Paper I) and for a tapering $f = 0.4, 0.65, 0.8$ are shown by the thick solid, dashed, thin solid and dotted curves respectively.

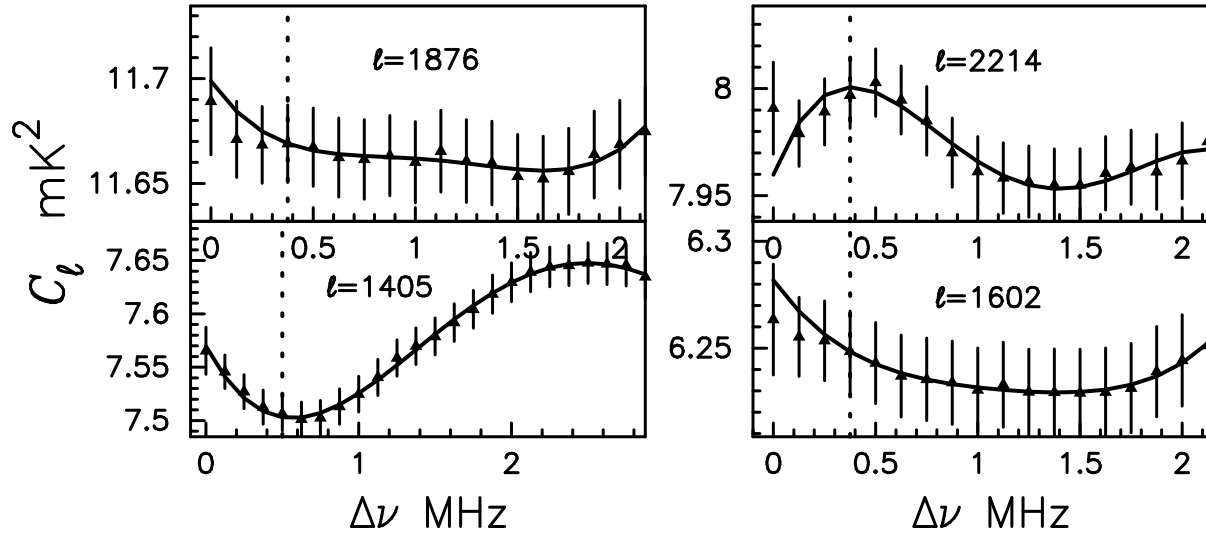


Figure 3. The data points show the measured $C_\ell(\Delta\nu)$ as a function of $\Delta\nu$ for the ℓ value shown in each panel. The error-bars indicate the 3σ system noise. The solid curve shows the 4^{th} order polynomial fits and the dotted vertical line shows $\Delta\nu_{0.1}$.

excluded in the likelihood analysis. The covariance between $C_\ell(\Delta\nu)$ at different $\Delta\nu$ values was taken into account in estimating the likelihood. We place an upper limit $\bar{x}_{\text{HIB}} \leq 2.9$ with 99% confidence using our observational data. In Paper I a high-pass filter had been applied to remove the oscillatory pattern at a single ℓ value (the smallest) to give an upper limit of 7.95 for \bar{x}_{HIB} . Table 1 summarizes the results of the current work, and presents a comparison with the results of Paper I. It is clear that the present analysis is a considerable improvement over the previous result. In conclusion we show that sidelobe suppression can bring about a considerable improvement in foreground removal.

4 ACKNOWLEDGMENT

We would like to thank the anonymous referee for providing us with constructive suggestions which helped to im-

Table 1. We show $\Delta C_\ell(\Delta\nu = 0)$, the $1 - \sigma$ error, for the ℓ values where it was possible to successfully remove the foregrounds. The upper limits on \bar{x}_{HIB} from the single ℓ value in Paper I and from combining the three different ℓ values in the current work are also shown.

ℓ	$\Delta C_\ell(\Delta\nu = 0)$ mK ²	\bar{x}_{HIB} 99% confidence
(Paper I)		
1476	0.010	≤ 7.95
(Current work)		
1405	0.007	
1602	0.008	≤ 2.9
1876	0.008	

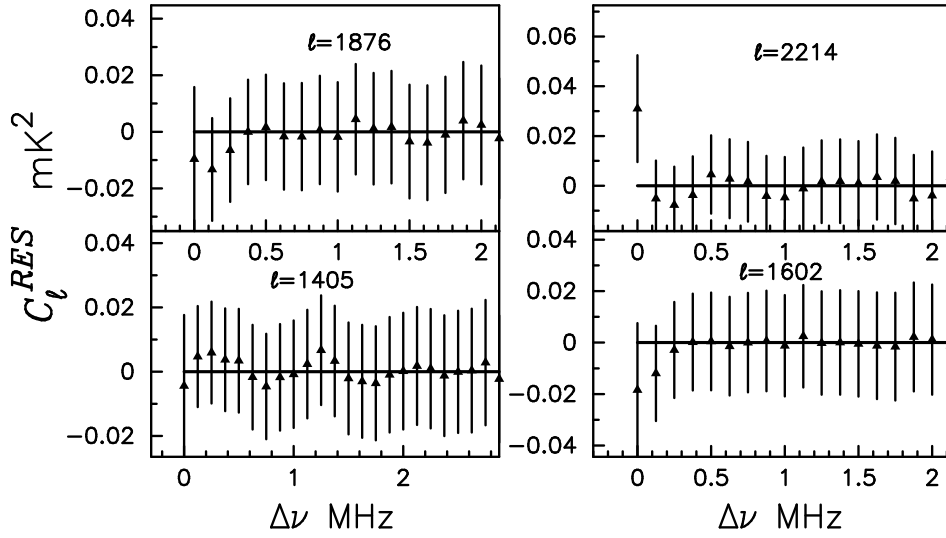


Figure 4. The residuals are shown with 3σ error bars (system noise only).

prove the paper. The authors would like to thank Ravi Subrahmanyan for pointing out the side-lobe effect during a workshop at HRI, Allahbad . AG thanks S.P. Khastgir for a detailed reading of the manuscript. AG acknowledges the Council of Scientific and Industrial Research (CSIR), India for financial support through Senior Research Fellowship (SRF). SSA would like to acknowledge CTS, IIT Kharagpur for the use of its facilities and the Associateship Programme of IUCAA for providing support. The data used in this paper was obtained using GMRT. The GMRT is run by the National Centre for Radio Astrophysics of the Tata Institute of Fundamental Research. We thank the GMRT staff for making these observations possible.

REFERENCES

- Ali S. S., Bharadwaj S., & Chengalur J. N., 2008, MNRAS, 385, 2166A
- Bharadwaj S., & Ali S. S. 2005, MNRAS, 356, 1519
- Bernardi, G., et al. 2009, Astronomy and Astrophysics, 500, 965
- Begum, A., Chengalur, J. N., & Bhardwaj, S. 2006, MNRAS, 372, L33
- Bharadwaj S., & Sethi S. K. 2001, Journal of Astrophysics and Astronomy, 22, 293
- Cohen, A. S., Röttgering, H. J. A., Jarvis, M. J., Kassim, N. E., & Lazio, T. J. W. 2004, ApJS, 150, 417
- Di Matteo, T., Perna R., Abel T. & Rees M.J., 2002, ApJ, 564, 576
- Di Matteo, T., Ciardi, B., & Miniati, F. 2004, MNRAS, 355, 1053
- Garn T., Green D. A., Riley J. M., & Alexander P. 2008, MNRAS, 387, 1037
- Gleser, L., Nusser, A., & Benson, A. J. 2008, MNRAS, 391, 383
- Ghosh, A., Bharadwaj, S., Ali, S. S., & Chengalur, J. N. 2011, MNRAS, 411, 2426
- Hales, S. E. G., Baldwin, J. E., & Warner, P. J. 1988, MNRAS, 234, 919
- Harker, G., et al. 2009, MNRAS, 397, 1138
- Haslam C. G. T., Salter C. J., Stoffel H., Wilson W. E., 1982, A&AS, 47, 1.
- Jonas, J.L., Baart, E.E., Nicolson, G.D., 1998, MNRAS, 297, 977.
- Jelić V., et al. 2008, MNRAS, 389, 1319
- Datta K. K., Roy Choudhury, T., & Bharadwaj. S, 2007, MNRAS, 378, 119
- Laing, R. A., Riley, J. M. & Longair, M. S. 1983, MNRAS, 204, 151
- Liu A., Tegmark M., Bowman J., Hewitt J., & Zaldarriaga M. 2009, arXiv:0903.4890
- Liu A., Tegmark M., & Zaldarriaga M. 2009, MNRAS, 394, 1575
- McQuinn M., Zahn O., Zaldarriaga M., Hernquist L. & Furlanetto S. R., 2006, ApJ, 653, 815
- Morales, M. F., & Hewitt, J. 2004, ApJ, 615, 7
- Petrovic, N., & Oh, S. P. 2011, MNRAS, 292
- Oh S. P., & Mack K. J. 2003, MNRAS, 346, 871
- Platania, P., Bensadoun, M., Bersanelli, M., de Amici, G., Kogut, A., Levin, S., Maino, D., & Smoot, G. F. 1998, ApJ, 505, 473
- Reich, W., 1982, A&AS, 48, 219.
- Reich, P. & Reich, W., 1988, A&AS, 74, 7.
- Santos M. G., Cooray A., & Knox L. 2005, ApJ, 625, 575
- Shaver, P. A., Windhorst, R. A., Madau, P., & de Bruyn, A. G. 1999, A & A, 345, 380
- Sramek A. R., & Schwab R. F., 1989, in Perley, R. A., Schwab, F. R., & Bridle, A. H., eds, ASP Conference Series, Synthesis Imaging in Radio Astronomy, Volume 6, p. 117
- Subrahmanyan, R. 2002, in IAU Symposium, Vol. 199, The Universe at Low Radio Frequencies, ed. A. Pramesh Rao, G. Swarup, & Gopal-Krishna, 58
- Swarup, G., Ananthakrishnan, S., Kapahi, V. K., Rao, A. P., Subrahmanya, C. R., & Kulkarni, V. K. 1991, CURRENT SCIENCE V.60, NO.2/JAN25, P. 95, 1991, 60, 95
- Wang X., Tegmark M., Santos M., & Knox, L., 2006, ApJ, 650, 529
- Zaldarriaga M., Furlanetto S. R., & Hernquist, L. 2004, ApJ, 608, 622